Analytical Debye-Huckel Model for Electrostatic Potentials around Dissolved DNA

Katrina Wagner, Edward Keyes, Thomas W. Kephart, and Glenn Edwards
Department of Physics and Astronomy, Vanderbilt University, Nashville, Tennessee 37235 USA

ABSTRACT We present an analytical, Green-function-based model for the electric potential of DNA in solution, treating the surrounding solvent with the Debye-Huckel approximation. The partial charge of each atom is accounted for by modeling DNA as linear distributions of atoms on concentric cylindrical surfaces. The condensed ions of the solvent are treated with the Debye-Huckel approximation. The resultant leading term of the potential is that of a continuous shielded line charge, and the higher order terms account for the helical structure. Within several angstroms of the surface there is sufficient information in the electric potential to distinguish features and symmetries of DNA. Plots of the potential and equipotential surfaces, dominated by the phosphate charges, reflect the structural differences between the A, B, and Z conformations and, to a smaller extent, the difference between base sequences. As the distances from the helices increase, the magnitudes of the potentials decrease. However, the bases and sugars account for a larger fraction of the double helix potential with increasing distance. We have found that when the solvent is treated with the Debye-Huckel approximation, the potential decays more rapidly in every direction from the surface than it did in the concentric dielectric cylinder approximation.

INTRODUCTION

Electrostatic interactions play a critical role in many fundamental biochemical, intermolecular processes (Anderson and Record, 1990; Davis and McCammon, 1990; Sharp and Honig, 1990a; Honig and Nicholls, 1995). The electrostatic properties of DNA are important in DNA-DNA (Vologodskii and Cozzarelli, 1994; Duguid and Bloomfield, 1996) and protein-DNA interactions (Misra et al., 1994a,b), as well as in determining the nature and structure of the condensed counterions around DNA (Manning, 1978; Mills et al., 1985; Fenley et al., 1990; Klement et al., 1991; Stigter, 1995). As such, the electric fields and potentials of DNA, and the details of the DNA-solvent interface, have been the subject of a great deal of theoretical research as well as comparison to experimental measurements of the electrostatic potential (Shin and Hubbell, 1992; Hecht et al., 1995). These investigations are relevant to experimental efforts to image DNA (Lyubchenko et al., 1992, 1993; Lee et al., 1994) and measurements of DNA-DNA repulsive forces (Rau and Parsegian, 1992).

Electrostatic models of the DNA-solvent system necessarily include idealizations due to the complexity of the system. Past investigations have used idealized geometries and charge distributions (Hill, 1955; Stigter, 1975; Schellman, 1977; Weisbuch and Gueron, 1981), and idealized models for the dielectric constant, ranging from no distinction between the inside and the outside of the macromolecule to a distant-dependent, composite dielectric function (Pullman and Pullman, 1981; Klein and Pack, 1983; Pack and Klein, 1984; Hingerty et al., 1985; Pack et al., 1990, 1993; Edwards et al., 1994; Lin-Chung and Rajagopal, 1995; Hochberg et al., 1997).

To account for the contribution of the counterions to the potential, many of the theoretical treatments of the potentials and the counterion concentrations make use of some form of the Poisson-Boltzmann equation, including the full nonlinear equation, its series approximation, and its linearized form, known as the Debye-Huckel model (Soumpasis, 1978; Pack et al., 1986; Gilson et al., 1987; Jayaram et al., 1989; Jayaram and Beveridge, 1990; Sharp and Honig, 1990b). Linearization of the Poisson-Boltzmann equation, invalid when the electrostatic energies are not much smaller than the thermal energies, conveniently allows the use of the superposition principle for the electrostatic potentials.

There have been several theoretical methods developed to calculate the potentials based on an all-atom model for DNA. Notably, Klein and Pack (1983; Pack and Klein, 1984) have calculated the potentials using an iterative method based on Coulomb's law and the Poisson-Boltzmann equation to determine a self-consistent set of potentials and ion concentrations. Jayaram et al. (1989) have also used an all-atom model to determine the electrostatic potential of B-DNA by using a finite-difference method to solve the nonlinear Poisson-Boltzmann equation. Later, Jayaram and Beveridge (1990) analytically solved the linearized Poisson-Boltzmann equation (Debye-Huckel approximation) for a finite length of DNA to determine the free energies of various conformations.

Hochberg et al. (1994) analytically determined the electrostatic potentials and fields around DNA in a phosphate-only, dielectric-layer model using a Green-function technique and later extended the model to include all of the atoms of DNA (Edwards et al., 1994). The method incorporates the symmetries of DNA; in particular, the atoms of DNA will form sets of parallel lines on the surfaces of concentric cylinders (Record, 1967). The solvent was

Received for publication 31 October 1996 and in final form 2 April 1997.
Address reprint requests to Dr. Glenn Edwards, Department of Physics and Astronomy, Vanderbilt University, Nashville, TN 37235. Tel.: 615-343-6440; Fax: 615-341-1103; E-mail: edwardg1@ctrvax.vanderbilt.edu.

0006-3495/97/07/21/10 $2.00

treated as a uniform dielectric medium. Bailey (1973) performed a similar calculation of the potential on the inside of DNA, accounting for the surrounding solvent in the Debye-Huckel approximation, but including only the phosphate charges.

Here we extend the all-atom analytical method to account for the surrounding counterions through the Debye-Huckel approximation, where the use of the linearized equation maintains the validity of the superposition principle. In addition, the present work also applies the theory to various conformations and sequences. Furthermore, we report a computational method for visualizing the analytical expressions for the electrostatic potential, based on color-coded cylinders in three dimensions, coaxial with a rendering of DNA.

THEORY

The general approach can be introduced by first considering just the phosphate charges associated with a single DNA strand (Hochberg et al., 1994). These charges lie along a single helix contained on a cylindrical surface centered about the longitudinal axis of an infinite, straight DNA molecule. It is advantageous to recast the geometry of this helix of discrete charges to account for the atoms by viewing them as a set of parallel lines, each containing charges separated by the helix pitch.

The potential due to each line of discrete charges can be readily calculated by summing the potentials of the series of point charges on the line; this is the merit of the alternative geometry. The potential due to all of the lines of discrete charges can then be summed, giving the potential due to the phosphates of a single strand of DNA. A similar process accounts for the phosphate charges of the complementary strand, where the symmetries of DNA simplify the forms of the resulting analytical expressions. This approach was then generalized for an all-atom model (Edwards et al., 1994), because the atoms of the sugars and bases can also be treated as described above.

In this paper we treat the solvent in a more sophisticated manner, replacing the uniform external dielectric layer with the Debye-Huckel formalism. The model of DNA in a 10 mM NaCl solution is depicted in Fig. 1 and consists of three cylindrically concentric regions. The radius of the inner cylinder, a_i, varies with the atom of interest, and its surface contains the line of charge associated with that atom. Region II extends from the surface of the inner cylinder to the surface of DNA at $\rho = b$. The outer region contains the condensed counterions; it has been proposed that the concentration in this region will vary with conformation (Manning, 1978; Klement et al., 1991). To determine the potential of a point charge, Poisson's equation,

$$\nabla^2\phi = -4\pi\rho_f/\epsilon_1 \qquad (1)$$

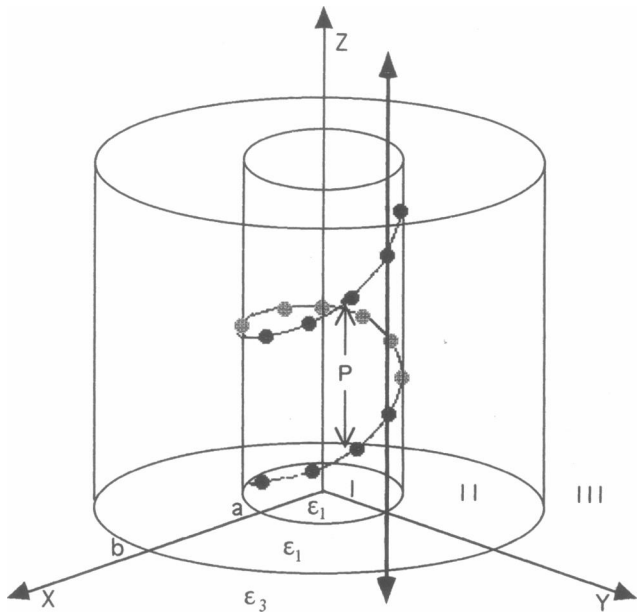

FIGURE 1 Geometry of the DNA-solvent system. The outer cylindrical surface represents the DNA surface, which lies just beyond phosphate groups. The inner cylindrical surface contains a helix of one type of interior atom, e.g., C_1' of the sugar group. The heavy line indicates one line of discrete charges. *P* indicates the helix pitch. Regions I and II have the same dielectric properties in this model. Region III corresponds to the condensed layer of counterions and is treated with the Debye-Huckel model.

is solved in regions I and II (see Fig. 1), where $\epsilon_1 = 2$ is the dielectric constant of these two regions and ρ_f accounts for the fixed discrete charges. The Debye-Huckel equation has the conveniently simple form

$$(\nabla^2 - \chi^2)\phi = -4\pi\rho_f/\epsilon_3 \qquad (2)$$

and is solved in region III, where ρ_f is again the fixed charge density. χ^{-1}, the Debye length, is determined by ϵ_3, the dielectric constant of the region outside DNA, and the counterion concentration calculated from the predictions of condensation theory (Manning, 1978). More specifically, we have modeled the solvent to account for partial dielectric saturation of water (Stogryn, 1971), recognizing that condensation increases the counterion concentration; the resulting potentials vanish at ~20 Å as expected. The parameters for the model calculations are listed in Table 1. Using the Green-function formalism (Jackson, 1975) and expanding in cylindrical coordinates (Hochberg et al., 1994), for a

TABLE 1 Model parameters for the solvent

Conformation	B	B′	A	Z
Counterion concentration (M)	1.2	1.32	2.59	0.95
Dielectric constant	59.2	57.7	44.2	62.5
Debye length (Å)	2.4	2.3	1.4	2.8

single charge at (ρ', φ', z'), Eq. 1 becomes

$$\nabla^2 G(x, x') = \frac{-4}{\pi\epsilon_1\rho}\delta(\rho - \rho')\int_0^\infty \cos k(z - z')\,dk \cdot \sum_{m'=0}^{\infty} \cos m(\varphi - \varphi') \tag{3}$$

and Eq. 2 becomes

$$(\nabla^2 - \chi^2)G(x, x') = \frac{-4}{\pi\epsilon_3\rho}\delta(\rho - \rho')\int_0^\infty \cos k(z - z')\,dk \cdot \sum_{m'=0}^{\infty} \cos m(\varphi - \varphi') \tag{4}$$

where the primed coordinates are those of the fixed charges and the prime on the sum over m indicates division of the zero ($m = 0$) term by 2 to avoid overcounting. We have taken the coordinates for the atoms from x-ray studies (Arnott and Hukins, 1972; Wang et al., 1981; Chandrasekaran et al., 1989; Chandrasekaran and Radha, 1992).

The solutions to Eq. 3 will be of the form

$$G(x, x') = \frac{1}{\pi^2}\sum_{m'=0}^{\infty}\int_0^\infty \cos m(\varphi - \varphi')\cos k(z - z')g_m(k, \rho, \rho')\,dk \tag{5}$$

where g_m is a function of the modified Bessel functions $K_m(k\rho)$ and $I_m(k\rho)$. The solutions of Eq. 4 will be of the form

$$G(x, x') = \frac{1}{\pi^2}\sum_{m'=0}^{\infty}\int_0^\infty \cos m(\varphi - \varphi')\cos k(z - z')g_m^{DH}(k, \rho, \rho')\,dk \tag{6}$$

where g_m^{DH} is still a function of the modified Bessel functions, but the arguments of the Bessel functions will now be $\rho\sqrt{k^2 + \chi^2}$, as discussed by Soumpasis (1978). In the limit that $\chi \to 0$, the solutions of the Debye-Huckel equation reduce to those found by Edwards et al. (1994). Because the fixed charges here are the DNA charges, which are treated as point charges, the Green functions will be equivalent to the potentials. Using trigonometric addition formulas and extracting all of the constant terms, the general solutions for the point charge potential in the three regions are

$$\Phi_I = \sum_{m'=0}^{\infty}\int_0^\infty I_m(k\rho)(A_{m,k}\cos m\varphi + B_{m,k}\sin m\varphi) \cdot (\alpha_{m,k}\sin kz + \beta_{m,k}\cos kz)\,dk \tag{7}$$

$$\Phi_{II} = \sum_{m'=0}^{\infty}\int_0^\infty (r_{m,k}I_m(k\rho) + K_m(k\rho))(C_{m,k}\cos m\varphi + D_{m,k}\sin m\varphi)(\gamma_{m,k}\sin kz + \delta_{m,k}\cos kz)\,dk \tag{8}$$

$$\Phi_{III} = \sum_{m'=0}^{\infty}\int_0^\infty K_m(\rho\sqrt{k^2 + \chi^2})(E_{m,k}\cos m\varphi + F_{m,k}\sin m\varphi) \cdot (\lambda_{m,k}\sin kz + \mu_{m,k}\cos kz)\,dk \tag{9}$$

The usual boundary conditions on the electric field will exist at each of the two boundaries: the perpendicular components of the dielectric displacement will be discontinuous by the amount of the surface charge and the parallel components of the electric field will be continuous. These boundary conditions can be written as

$$\begin{aligned}
\epsilon_1\frac{\partial\Phi_I}{\partial\rho} - \epsilon_1\frac{\partial\Phi_{II}}{\partial\rho}\Big|_{\rho=a} &= 4\pi\sigma \\
\epsilon_1\frac{\partial\Phi_{II}}{\partial\rho} - \epsilon_3\frac{\partial\Phi_{III}}{\partial\rho}\Big|_{\rho=b} &= 0 \\
\frac{\partial\Phi_{II}}{\partial z} - \frac{\partial\Phi_I}{\partial z}\Big|_{\rho=a} &= 0 \\
\frac{\partial\Phi_{III}}{\partial z} - \frac{\partial\Phi_{II}}{\partial z}\Big|_{\rho=b} &= 0
\end{aligned} \tag{10}$$

where the charges of DNA on the inner surface, σ, will be represented by delta functions that can also be expanded in the same basis set as the Green function.

The constants of Eqs. 7–9 are determined by matching the boundary conditions of Eq. 10 such that the potentials due to a single charge of DNA become

$$\Phi_I = \sum_{m'=0}^{\infty}\int_0^\infty \frac{4q_i}{\pi\epsilon_1} I_m(k\rho)[r_{m,k}I_m(ka_i) + K_m(ka_i)] \cdot \cos k(z - z')\cos m(\varphi - \varphi')\,dk \tag{11}$$

$$\Phi_{II} = \sum_{m'=0}^{\infty}\int_0^\infty \frac{4q_i}{\pi\epsilon_1} I_m(ka_i)[r_{m,k}I_m(k\rho) + K_m(k\rho)] \cdot \cos k(z - z')\cos m(\varphi - \varphi')\,dk \tag{12}$$

and

$$\Phi_{III} = \sum_{m'=0}^{\infty}\int_0^\infty \frac{4q_i}{\pi\epsilon_3}\frac{K_m(\rho\sqrt{k^2 + \chi^2})I_m(ka_i)}{K_m(b\sqrt{k^2 + \chi^2})} \cdot [r_{m,k}I_m(kb) + K_m(kb)]\cos k(z - z')\cos m(\varphi - \varphi')\,dk \tag{13}$$

where q_i is the charge of the atom under consideration, the values for which are taken from Pearlman and Kim (1990), and

$$r_{m,k} = \frac{\epsilon_3\sqrt{k^2+\chi^2}K_m(kb)K_m'(b\sqrt{k^2+\chi^2}) - \epsilon_1 kK_m'(kb)K_m(b\sqrt{k^2+\chi^2})}{\epsilon_1 kI_m'(kb)K_m(b\sqrt{k^2+\chi^2}) - \epsilon_3\sqrt{k^2+\chi^2}I_m(kb)K_m'(b\sqrt{k^2+\chi^2})} \quad (14)$$

The primes on the Bessel functions indicate differentiation with respect to their arguments.

The $m = 0$ and $k = 0$ terms must be pulled out and treated individually because of the special forms of zero-order Bessel functions and Bessel functions of argument zero (Abramowitz and Stegun, 1970). The z position of the nth charge of type i on the sth line is $z' = z_i + nP + s\Delta z$, where P is the pitch of the helix, Δz is the rise per base pair, and z_i is the coordinate of the first atom above the $z = 0$ plane on the $s = 0$ line. Summing the charges on a line will then create a sum over n. If N is the number of bases per turn, then there are $s = N$ strands, each located at $\varphi' = \varphi_i + 2\pi s/N$ (for a right-handed helix), where φ_i is the φ coordinate of the first charge of type i on the $s = 0$ line. Summing the lines on the cylindrical surface will then create a sum over s.

Several identities derived from the Poisson summation formula (Lighthill, 1970) will simplify the equations containing the n and s sums by introducing delta functions into the integrals:

$$\sum_{n=-\infty}^{\infty}\cos k(z - z_i - np - s\Delta z)$$

$$= \frac{2\pi}{P}\cos k(z - z_i - s\Delta z)\sum_{j=-\infty}^{\infty}\delta\left(k - \frac{2\pi j}{P}\right)$$

$$\sum_{s=0}^{N-1}\cos\left(\frac{2\pi j}{P}(z - z_i - s\Delta z)\right) = N\cos\left(\frac{2\pi j(z - z_i)}{P}\right)\delta_{j,\ell N}$$

$$\sum_{s=0}^{N-1}\cos\left(m\left(\varphi - \varphi_i - \frac{2\pi s}{N}\right)\right) = N\cos(m\varphi - m\varphi_i)\delta_{m,\ell N}$$

$$\sum_{s=0}^{N-1}\cos\left(\frac{2\pi j}{P}(z - z_i - s\Delta z)\right)\cos\left(m\left(\varphi - \varphi_i - \frac{2\pi s}{N}\right)\right)$$

$$= \frac{N}{2}\cos\left(\frac{2\pi j(z - z_i)}{P} + m(\varphi - \varphi_i)\right)\delta_{(j+m),\ell N}$$

$$+ \frac{N}{2}\cos\left(\frac{2\pi j(z - z_i)}{P} - m(\varphi - \varphi_i)\right)\delta_{(j-m),\ell N} \quad (15)$$

where $-\infty < \ell < \infty$. After some tedious but straightforward algebra, the potential due to an entire right-handed single helix on the outside of the helix, which is the region of interest to us, can be written as

$$\Phi_{IIIh} = \sum_i\left\{\frac{-2q_iK_0(\chi\rho)}{b\Delta z\epsilon_3\chi K_0'(\chi b)} + \sum_{j=1}^{\infty}\frac{4q_i}{b\Delta z}K_0\left(\rho\sqrt{\left(\frac{2\pi j}{\Delta z}\right)^2+\chi^2}\right)\right.$$
$$\cdot\cos\left(\frac{2\pi j(z - z_i)}{\Delta z}\right)\Omega\left(0, \frac{2\pi j}{\Delta z}\right) + \sum_{j=1}^{\infty}\frac{4q_i}{\Delta z}$$
$$\cdot\cos(jN(\varphi - \varphi_i))\frac{a_i^{jN}K_{jN}(\chi\rho)}{b^{jN}(jN\epsilon_1K_{jN}(\chi b) - b^{-1}\epsilon_3\chi K_{jN}'(\chi b))}$$
$$+ \sum_{j=1}^{\infty}\sum_{m=1}^{jN-1}\frac{4q_i}{\Delta z b}K_m\left(\rho\sqrt{\left(\frac{2\pi(jN-m)}{P}\right)^2+\chi^2}\right)$$
$$\cdot\Omega\left(m, \frac{2\pi}{P}(jN - m)\right) \quad (16)$$
$$\cdot\cos\left(\frac{2\pi(z - z_i)}{P}(jN - m) + m\varphi - m\varphi_i\right)$$
$$+ \sum_{j=-\infty}^{\infty}\sum_{m=\max[1,1-jN]}^{\infty}\frac{4q_i}{\Delta z b}K_m\left(\rho\sqrt{\left(\frac{2\pi(jN+m)}{P}\right)^2+\chi^2}\right)$$
$$\cdot\Omega\left(m, \frac{2\pi}{P}(jN + m)\right)$$
$$\left.\cdot\cos\left(\frac{2\pi(z - z_i)}{P}(jN + m) - m\varphi + m\varphi_i\right)\right\}$$

where

$$\Omega(m, k) = \frac{I_m(ka_i)}{\epsilon_1 kI_m'(kb)K_m(b\sqrt{k^2+\chi^2}) - \epsilon_3\sqrt{k^2+\chi^2}I_m(kb)K_m'(b\sqrt{k^2+\chi^2})} \quad (17)$$

For a left-handed helix, the $m\varphi$ terms that appear in the cosines of the last two terms of the potential will change sign. The first term of Eq. 16, corresponding to the $m = 0$, $k = 0$ case, is equivalent to the potential of a uniformly charged cylinder using the Debye-Huckel approximation (Hill, 1955). The higher order terms will contribute helical structure to the potential.

RESULTS

The potentials were calculated and rendered using the program BlueGenes, described in the Appendix. A copy of the BlueGenes software is available upon request from the

Vanderbilt Department of Physics and Astronomy WWW site http://comped1.cas.vanderbilt.edu/.

Fig. 2 *a* shows the potential around B-DNA polyd(AT)-polyd(AT) based on Eq. 16. For comparison, Fig. 2 *b* also shows the potential around B-DNA polyd(AT)-polyd(AT), but calculated from the equations of Edwards et al. (1994), which treat the solvent as a uniform dielectric medium. The introduction of the Debye-Huckel approximation screens the charges of the DNA, leading to enhanced contrast, and as expected, the potential is smaller when the Debye-Huckel approximation is used.

Fig. 3 shows the potentials due to just the bases of B-DNA polyd(AT)-polyd(AT), B′-DNA polyd(A)-polyd(T) (Chandrasekaran and Radha, 1992), A-DNA polyd(G)-polyd(C), and Z-DNA polyd(GC)-polyd(GC). The potential shells are 1 Å from the atom of the helix with the largest radial coordinate. All of the base potentials show regions of positive and negative potential, reflecting the spatial arrangements of the partial charges within the bases.

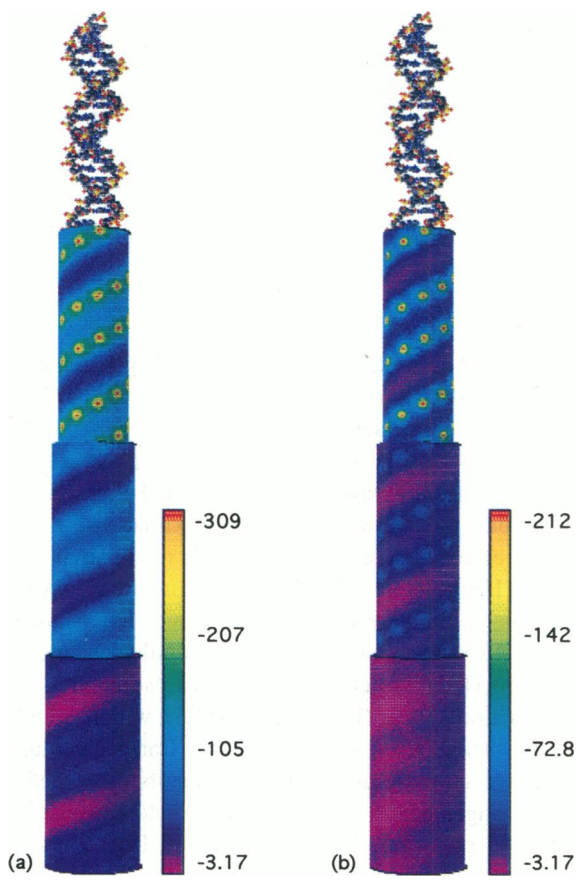

FIGURE 2 (*a*) The potentials around B-DNA polyd(AT)-polyd(AT), found by using a uniform dielectric layer approximation (Edwards et al., 1994). (*b*) The potentials found from Eq. 16 around B-DNA polyd(AT)-polyd(AT). The shells are located at 11.2 Å, 13.2 Å, and 15.2 Å, or equivalently, 1 Å, 3 Å, and 5 Å from the charge having the largest radial coordinate. The scales give the potentials in millivolts. The scale in *a* has been renormalized because the potential around an infinite unshielded line charge will tend to infinity as ρ approaches infinity.

The negative (*orange*) regions of the B′-DNA polyd(A)-polyd(T) lie toward the adenine side of the minor groove, and the positive (*purple*) regions are toward the thymine side of the major groove. The bases of this conformation contain no noticeable structure along the grooves. In the B-DNA polyd(AT)-polyd(AT) helix the negative regions are also in the minor groove, and the positive regions, because of the methyl group of the thymine, are on the outer edge of the major groove. The minor groove of the A-DNA contains the negative regions, where the more negative side corresponds to the cytosine strand. The potential due to the bases of Z-DNA is the strongest and shows the most structure, because the bases of this conformation lie very close to the surface of the molecule. The positive features are chiefly due to the C8 atom of the guanine, and the alternating regions of negative structure are due mostly to the N1 atoms of the cytosine.

Fig. 4 shows the potentials due to all of the atoms of the double helix for the same conformations and sequences for which the base potentials were shown. Once again, the shells are located 1 Å from the helix charge with the largest radial coordinate. It is obvious from comparing Fig. 4 to Fig. 3 that the bases are a small contributor to the overall double-helix potential. The large negative regions correspond to the phosphate groups and accurately reflect the groove sizes.

Neither the B-DNA polyd(AT)-polyd(AT) nor the B′-DNA polyd(A)-polyd(T) helix has regions of positive potential. The contribution of the bases' potentials to both of these helices increases the magnitude of the negative potential in the minor groove. For the potential plot of B′-DNA polyd(A)-polyd(T) double helix, the more negative of the two phosphate strands corresponds to the thymine strand, which has larger radial coordinates than the phosphate strand attached to the adenines.

The positive (*purple*) regions that appear on the plot of the A-DNA potential come from the sugar groups, which are displaced in the z direction from the phosphates, as can be determined by examining a plot of the potential due only to the bases and phosphates (data not shown), where this structure no longer exists. The minor groove of the A-DNA is made more negative by the presence of the bases, whereas the region of the major groove is made slightly more positive.

Only every other phosphate of the Z-DNA is easily seen, because alternating phosphates are recessed in the ρ direction. The positive regions in the potential of the Z-DNA double helix are due to both the sugars and the bases. By comparing the potential of the backbone to that of the double helix, it can be seen that the Z-DNA bases make the potential in the areas around the phosphates more negative and the potential in the minor groove more positive.

In all cases the phosphate groups are the strongest contributors to the double-helix potentials. Because the phosphate groups carry the largest charge and are closest to the surface of the molecule, the potential due to these groups will initially fall off faster with ρ (starting from the molecule's surface) than the potentials due to the bases or sugars.

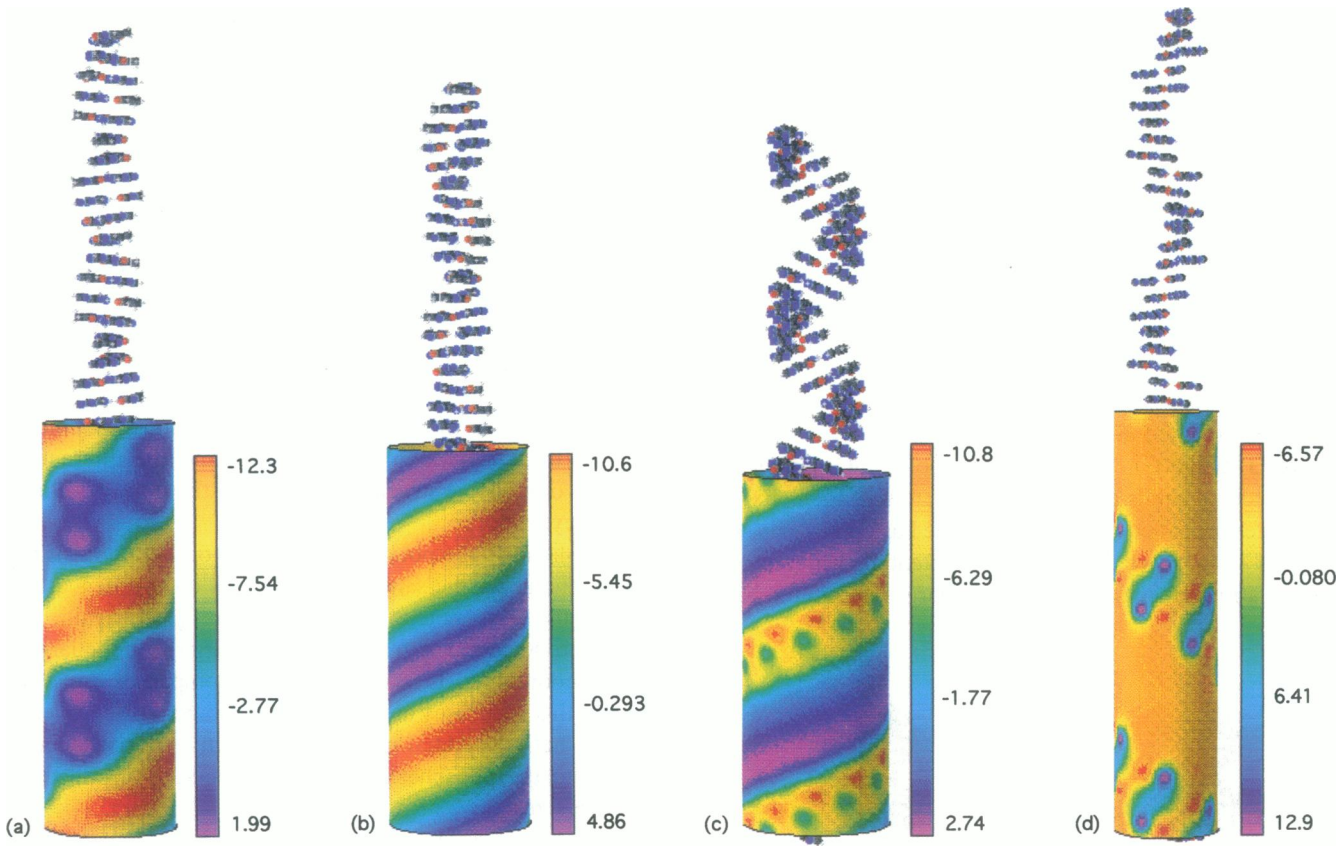

FIGURE 3 The potentials due to the bases of (*a*) B-DNA polyd(AT)-polyd(AT) at 11.2 Å; (*b*) B′-DNA polyd(A)-polyd(T) at 11.9 Å; (*c*) A-DNA polyd(G)-polyd(C) at 11.6 Å; and (*d*) Z-DNA polyd(GC)polyd(GC) at 9.8 Å. The distances correspond to 1 Å from the charge having the largest radial coordinate in the given helix. The numbers on the scale are given in millivolts.

Farther from the DNA, where the decay and strength of the phosphate potentials are less dramatic, the potentials of the charges in the bases or sugars can contribute a larger percentage to the overall double helix potential relative to their contribution closer to the double helix, where their potentials were still overshadowed by the phosphates. When the potentials are viewed farther from the helices (at ~17 Å from the helix center), the same general structure still exists but is much weaker (where the difference between the maximum and minimum potentials is only several millivolts) and more diffuse, and there are no longer positive regions in the double-helix potentials, supporting the idea that far from the helix the model of a uniformly charged cylinder can adequately describe the system. However, as stated before, the bases and sugars contribute slightly more to the overall potential at greater distances.

Equipotential surfaces around B-DNA polyd(AT)-polyd(AT) are shown in Fig. 5. The inner surface is located at 1 *kT* and the outer surface at 0.1 *kT*. The flat red regions are areas where the potential is either positive or, at the helix surface, already less than the potential of the equipotential surface.

These results should be compared with those of previous model calculations. The linearization resulting from the Debye-Huckel approximation is not strictly justifiable for a highly charged polyion such as DNA. Stigter (1975) has tabulated correction factors to compensate for the nonlinear contribution, which is a smooth function of distance for a uniformly charged cylinder. Relative to the Poisson-Boltzmann model, the Debye-Huckel approximation underestimates the effect of screening and yields results that are too negative (Hecht et al., 1995). Furthermore, the Poisson-Boltzmann results are also too negative. This has been attributed to neglect of ion-ion core repulsions and ionic correlations (Klement et al., 1991) and to screening effects by the ion atmosphere (Hecht et al., 1995), which is claimed to be consistent with previous Monte Carlo calculations. These observations indicate that the results presented here are too strongly negative and underestimate contrast in the electrostatic potential. Nonetheless, from Fig. 5 it can be seen that our model predicts potentials 14 Å from the minor groove of B-DNA to be around -1 *kT*, apparently in better agreement with experiment (Shin and Hubbell, 1992; Hecht et al., 1995) than other Debye-Huckel calculations in 10 mM salt. Furthermore, Jayaram et al. (1989) examined the potential on the surfaces of B-DNA polyd(A)-polyd(T) and polyd(G)-polyd(C) using the Poisson-Boltzmann equation, finding patterns of positive and negative potential within the

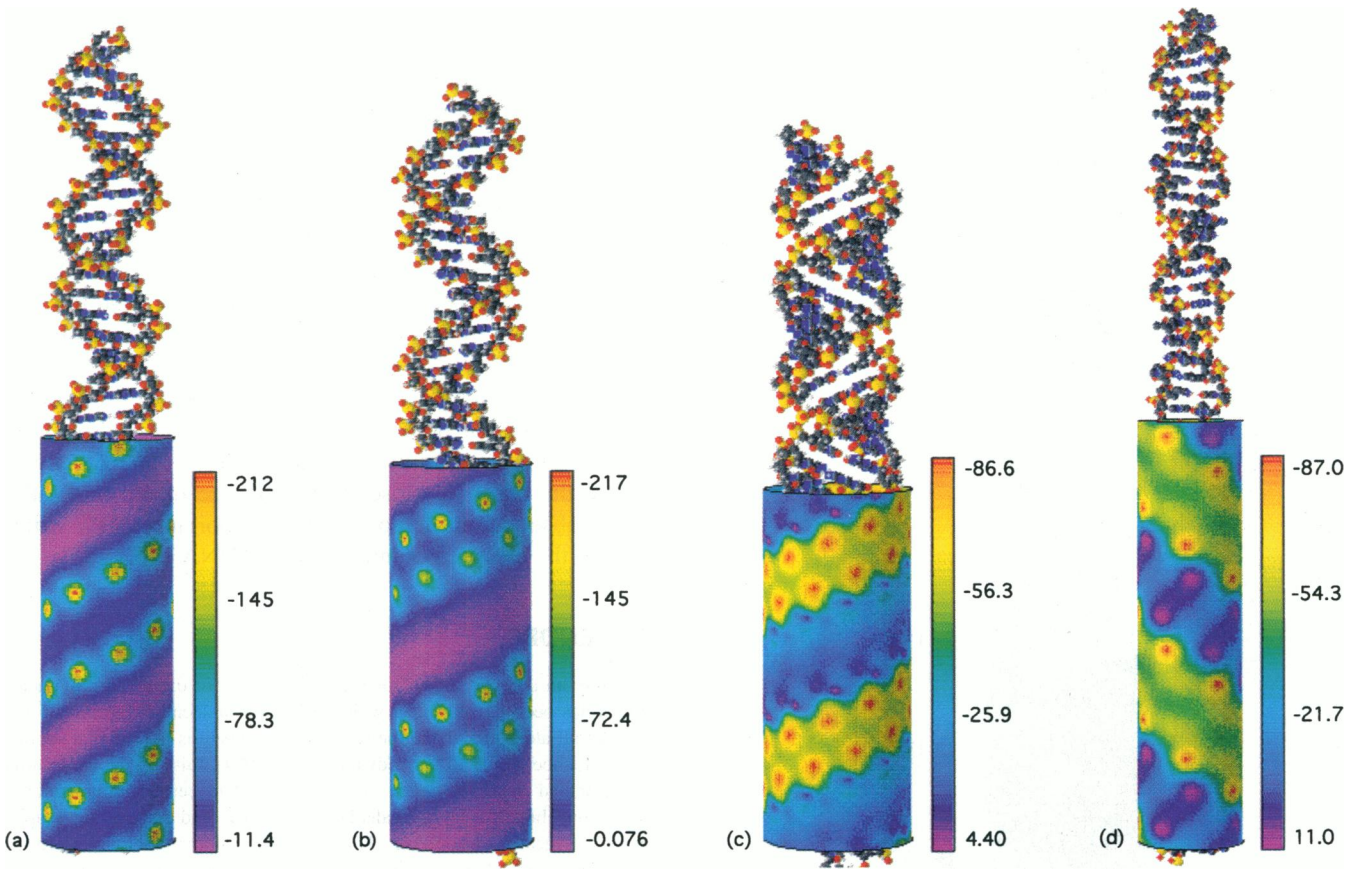

FIGURE 4 The potentials due to the double helices (*a*) B-DNA polyd(AT)-polyd(AT) at 11.2 Å; (*b*) B′-DNA polyd(A)-polyd(T) at 11.9 Å; (*c*) A-DNA polyd(G)-polyd(C) at 11.6 Å; and (*d*) Z-DNA polyd(GC)-polyd(GC) at 9.8 Å. The units of the scale are millivolts. The colored shells are located an angstrom from the charge of the helix with the largest radial coordinate.

grooves; there were regions of large negative potential in the minor grooves of both sequences and on the guanine side of the major groove of the polyd(G)-polyd(C). Our calculations for just the bases of polyd(G)-polyd(C) (data not shown) and polyd(A)-polyd(T) reveal the same patterns of negative and positive potential, although with less structure than that seen by Jayaram, because we are farther from the surface, suggesting that the structure in the potential near the surface indeed is due to the bases.

This version of a composite cylinder model neglects the effects of grooves, more specifically the effect on the dielectric constant in the region corresponding to the grooves. Computational models have investigated groove effects, finding a counterintuitive charge reversal effect in the solvent (Montoro and Abascal, 1995). In addition, calculations by Demaret and Gueron (1993) show that the phosphates of Z-DNA have fewer condensed ions relative to the phosphates of B-DNA, supporting the proposition that phosphate immersion is a key electrostatic contribution to the B-Z transition. In our Fig. 4, *a* and *d*, the potential surfaces are 2.45 Å from the (outer) phosphates: the potentials around the outer Z phosphates are less than half the magnitude of the potentials around the B phosphates, indicating that there will be more condensed ions around the phosphates of the B conformation. It should also be noted that the Z conformation is the only structure that shows substantial regions of positive potential.

Computational models indicate that the local ionic distribution indeed does depend on conformation, sequence, and salt concentration (Klement et al., 1991). Furthermore, unresolved issues regarding the mobility of water in the grooves adds to the ambiguity for the specific choice of dielectric constant for DNA systems. To test the sensitivity of our model to this choice, we have varied the dielectric constant for DNA. Whereas the qualitative pattern of the near field is unchanged, increasing the dielectric constant decreases the magnitude of the potential, with the strongest effects observed near the phosphate groups, as expected. More quantitatively, we compared the values 1, 4, 10, and 57.7 (no dielectric boundary) with the nominal value of 2 for the dielectric constant of the region corresponding to DNA (results not shown). The maximum effect was a 1% increase or a 2%, 7.6%, or 76% decrease, respectively. Thus, as found by Pack et al. (1993) and Jayaram et al. (1989), the inclusion of the dielectric boundary between the low dielectric region inside the molecule and the high

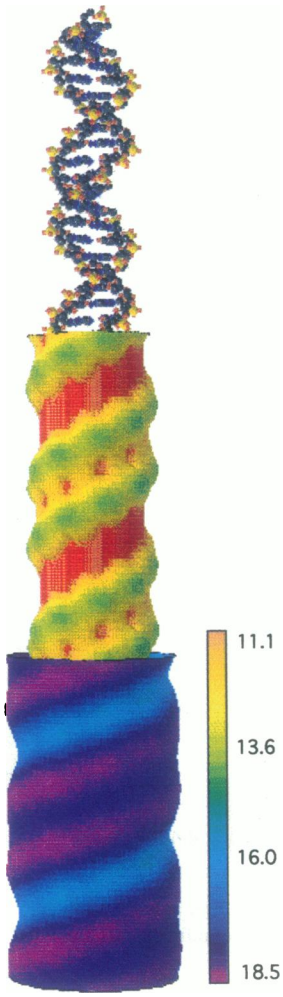

FIGURE 5 Equipotential surfaces around B-DNA polyd(AT)-polyd(AT). The inner surface is located at $1.0kT$ and the outer surface is at $0.1kT$. The scale bar gives the distance from the helix center in angstroms. The spatial position of the equipotential surface provides the same information as the colors.

dielectric region outside increases the magnitude of the calculated potential.

CONCLUDING REMARKS

The analytical model presented here makes it possible to view the potentials and counterion concentrations around various conformations and sequences of DNA in a clear and rapid manner. The use of the Debye-Huckel approximation is an improvement in the treatment of the solvent over the earlier calculations of Edwards et al. (1994). However, the treatment of the counterions through the Debye-Huckel approximation must be viewed as suspect close to DNA, where the electrostatic energy can be larger than the thermal energy. In the future we intend to recalculate the potentials using the full Poisson-Boltzmann equation (Garrett and Poladian, 1988). In addition, this version of a composite cylinder model ignores the effects of grooves and will not account for any focusing effects due to solvent penetration.

The conformation dependencies of the electric potentials around DNA are apparent in the plots of potential and equipotentials, notably through the potentials of the phosphates. The spatial arrangements of the partial charges of the bases produce sequence-dependent structure in the double-helix potential, as has been seen in other all-atom calculations of the potentials (Jayaram et al., 1989). However, these effects are often overshadowed in the double-helix potential by the significantly larger effects due to the phosphates. Farther from the helix, the magnitude of the potentials is much less, but the bases contribute proportionally more to the double-helix potential. These sequence-dependent affects are more obvious in the A and Z helices, where the bases lie closer to the surface of the molecule. These observations demonstrate the importance of the structure of the electric potential near the DNA surface.

APPENDIX

Recently an analytic model for the electrostatics of dissolved polynucleotides has been developed in which the DNA molecule is accounted for with an all-atom model and the surrounding solvent is treated as a continuum (Hochberg et al., 1994; Edwards et al., 1994). Initially the model was implemented in *Mathematica* and was subject to certain computational limitations. In particular, the calculation was slow, and the resulting graphs were not ideally informative. This appendix summarizes our efforts to upgrade the calculation engine, reducing the calculation time by several orders of magnitude to just minutes on a desktop computer. In addition, a visualization method has been developed to display these complex data sets in an easily understandable fashion, allowing direct comparison of conformations, sequences, various models of the solvent, etc. (Keyes, 1996). The current implementation of this visualization method accommodates any linear, periodic molecule with helical symmetry and is not model dependent. The method can be generalized to periodic, nonhelical molecules.

To overcome previous computational limitations, the calculation engine for the analytic model was reimplemented in C. Polynomial approximations and appropriate recursion formulas were used for the modified Bessel functions composing the equations (Press et al., 1995). In addition, symmetries in the equations themselves were exploited to avoid recalculation of functions over the course of evaluating multiple data points. The new calculation engine scales better than linearly with the number of data points, until overall loop structure combining intermediate results dominates the running time, at which point linear behavior is approached, as shown in Fig. 6. The net result was a speedup factor of ~8000 over the original *Mathematica* implementation. On a current entry-level Power Macintosh, this allows the full calculation of the electrostatic potential around DNA at better than atomic resolution in minutes or less. Because the analytic expressions are expressed in Fourier space, the spatial resolution is set by the truncation of the infinite sums present in the analytic solution: we generally work with finite sums corresponding to a resolution of 0.1 Å.

With such an excess of calculable data points, a more intuitive visualization method was both possible and necessary. Because of the symmetries in the analytic expressions, it was computationally advantageous to calculate data points on a regular lattice in cylindrical coordinates; this greatly influenced the resulting visualization method. An intuitive method for presenting electrostatic models of dissolved molecules can be based on renderings of the potential on cylindrical surfaces: data points evaluated on a regular grid at a constant distance from the symmetry axis of the molecule. To provide spatial cues, the surface is presented in 3D space, coaxial with a rendering of the molecule. The placement of the surface provides an in-scale indication of the distance at which the data points were evaluated. However, this approach reduces the number of dimensions

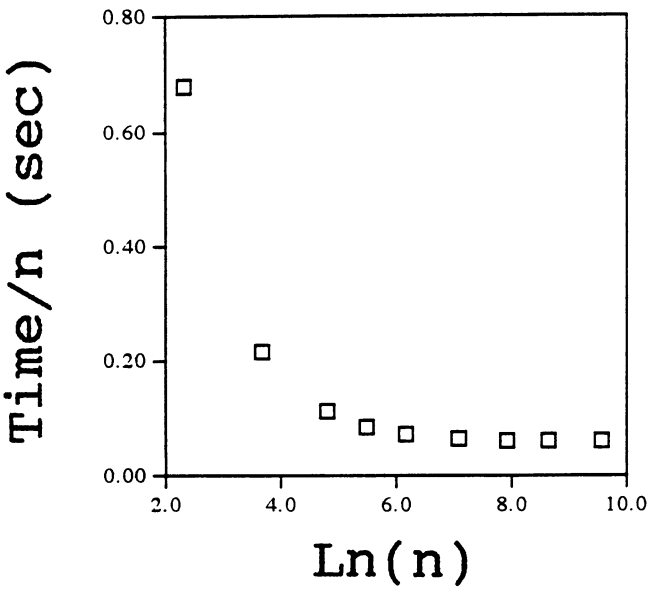

FIGURE 6 Timing trials for the BlueGenes computer program as implemented on a 80 MHz PowerMacintosh 6100. Average time required to calculate the potential at a given point in space for B-DNA. The calculation engine becomes more efficient with increasing number of data points n, limiting to a computation time of 0.057 s/data point when the loop structure saturates performance.

available to encode the actual data; consequently, color-coding the intensity of the potential was adopted.

The result is the visualization presented in Figs. 2–5 and 7: a cylindrical surface placed in space around a rendering of the molecule, color-coded with the electrostatic potential at that particular point. This method has several key advantages. It allows an immediate and intuitive matching of molecular structure to features in the electrostatic potential; for example, the influence of the highly charged phosphate groups is readily apparent. Because of the periodic grid of data points, the method is fast to calculate, and because of the simplicity of the 3D shapes used (flat-shaded spheres and texture-mapped cylinders), it is fast to render. The method is relatively simple, and thus is easy to implement for other models of the potential, on any platform in which basic 3D visualization tools are available.

Because the same points in space can be evaluated from run to run, data sets can be directly compared and subtracted, unlike the data from an equipotential surface. For example, the contribution from the ribose groups is clear from inspection of Fig. 7. The use of multiple cylindrical surfaces at different radii effectively portrays the falloff of electrostatic features with distance.

This visualization method has some limitations. The use of color-coding to represent data is necessarily less accurate than more traditional graphs, because of inherent inaccuracies in the reproduction of color by modern devices. The method may be less intuitive than an equipotential plot, but the use of color rather than shape to represent data gives finer levels of detail. A possible extension to the method for black-and-white format utilizing a contour plot of the potential mapped onto the cylindrical surface may mitigate the dependence on color without losing spatially intuitive features.

This visualization method, known locally by the program's name, BlueGenes, is model and platform independent, is quick to implement and render, and is visually intuitive. Although other electrostatic models may require the power of a workstation or even a supercomputer, implementing BlueGenes requires only a desktop computer, with all of the advantages of rapid feedback, and including the potential for animation. A copy of the BlueGenes software is available upon request from the Vanderbilt Department of Physics and Astronomy WWW site http://comped1.cas.vanderbilt.edu/.

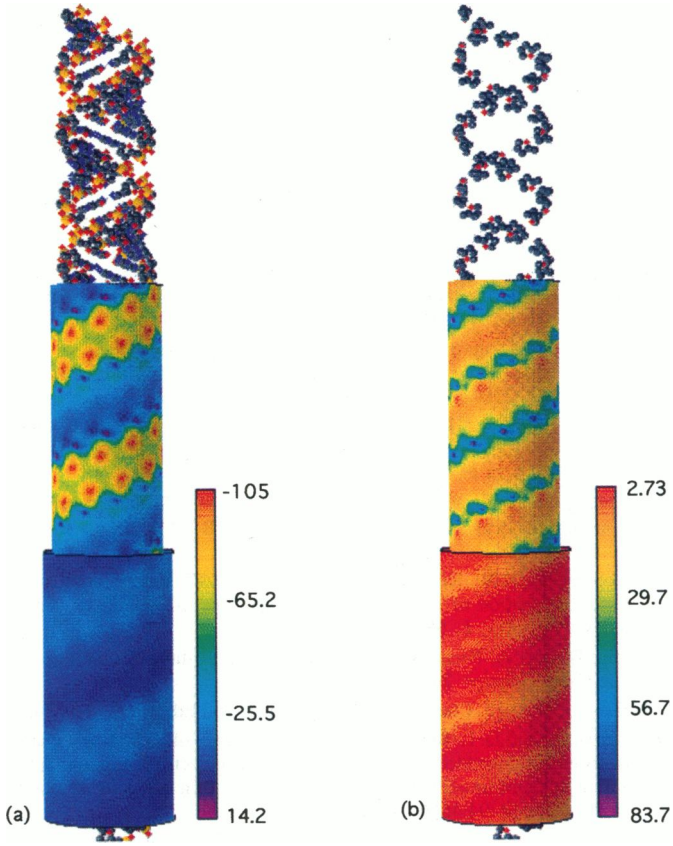

FIGURE 7 Potentials at 11.5 and 13.5 Å due to (*a*) all atoms of polyd(G)-polyd(C) A-DNA and (*b*) the contribution from the ribose groups only. The solvent is 10 mM NaCl. The units are millivolts.

This research was supported in part by Vanderbilt University and by the Department of Defense Medical Free-Electron Laser program through contract number ONR-N00014-91-0109.

REFERENCES

Abramowitz, M., and I. A. Stegun. 1970. Handbook of Mathematical Functions. Dover, New York.

Anderson, C. F., and M. T. Record, Jr. 1990. Ion distributions around DNA and other cylindrical polyions: theoretical descriptions and physical implications. *Annu. Rev. Biophys. Biophys. Chem.* 19:423–465.

Arnott, S., and D. W. L. Hukins. 1972. Optimised parameters for A-DNA and B-DNA. *Biochem. Biophys. Res. Commun.* 47:1504–1510.

Bailey, J. M. 1973. The electrostatic potential of a discretely charged cylinder in solution. *Biopolymers.* 12:559–574.

Chandrasekaran, R., and A. Radha. 1992. Structure of polyd(A)-polyd(T). *J. Biomol. Struct. Dyn.* 10:153–168.

Chandrasekaran, R., M. Wang, R.-G. He, L. C. Puigjaner, M. A. Byler, R. P. Millane, and S. Arnott. 1989. A re-examination of the crystal structure of A-DNA using fiber diffraction data. *J. Biomol. Struct. Dyn.* 6:1189–1202.

Davis, M. E., and J. A. McCammon, 1990. Electrostatics in biomolecular structure and dynamics. *Chem. Rev.* 90:509–521.

Demaret, J.-P., and M. Gueron. 1993. Composite cylinder models of DNA: application to the electrostatics of the B-Z transition. *Biophys. J.* 65: 1700–1713.

Duguid, J. G., and V. A. Bloomfield. 1996. Electrostatic effects on the stability of condensed DNA in the presence of divalent cations. *Biophys. J.* 70:2838–2846.

Edwards, G., D. Hochberg, and T. W. Kephart. 1994. Structure in the electric potential emanating from DNA. *Phys. Rev. E.* 50:R698–R701.

Fenley, M. O., G. S. Manning, and W. K. Olson. 1990. Approach to the limit of counterion condensation. *Biopolymers.* 30:1191–1203.

Garrett, A. J. M., and L. Poladian. 1988. Refined derivation, exact solutions, and singular limits of the Poisson-Boltzmann equation. *Ann. Phys.* 188:386–435.

Gilson, M. K., K. A. Sharp, and B. H. Honig. 1987. Calculating the electrostatic potential of molecules in solution: method and error assessment. *J. Comp. Chem.* 9:327–335.

Hecht, J. L., B. Honig, Y.-K. Shin, and W. L. Hubbard. 1995. Electrostatic potentials near the surface of DNA: comparing theory and experiment. *J. Phys. Chem.* 99:7782–7786.

Hill, T. L. 1955. Approximate calculation of the electrostatic free energy of nucleic acids and other cylindrical macromolecules. *Arch. Biochem. Biophys.* 57:229–239.

Hingerty, B. E., R. H. Ritchie, T. L. Ferrell, and J. E. Turner. 1985. Dielectric effects in biopolymers: the theory of ionic saturation revisited. *Biopolymers.* 24:427–439.

Hochberg, D., T. W. Kephart, and G. Edwards. 1994. Structural information in the local electric field of dissolved B-DNA. *Phys. Rev. E.* 49:851–867.

Hochberg, D., T. W. Kephart, and G. Edwards. 1997. Representing structural information of helical charge distributions in cylindrical coordinates. *Phys. Rev. E.* 55:3765–3768.

Honig, B., and A. Nicholls, 1995. Classical electrostatics in biology and chemistry. *Science.* 268:1144–1149.

Jackson, J. D. 1975. Classical Electrodynamics, 2nd Ed. Wiley, New York.

Jayaram, B., and D. L. Beveridge. 1990. Free energy of an arbitrary charge distribution imbedded in coaxial cylindrical dielectric continua: application to conformational preferences of DNA in aqueous solutions. *J. Phys. Chem.* 94:4666–4671.

Jayaram, B., K. A. Sharp, and B. Honig. 1989. The electrostatic potential of B-DNA. *Biopolymers.* 28:975–993.

Keyes, E. 1996. Computation and visualization of the electrostatic potential of DNA. Senior thesis, Vanderbilt University, Nashville, TN.

Klein, B. J., and G. R. Pack. 1983. Calculations of the spatial distribution of charge density in the environment of DNA. *Biopolymers.* 22: 2331–2352.

Klement, R., D. M. Soumpasis, and T. M. Jovin. 1991. Computation of ionic distributions around charged bimolecular structures: results for right-handed and left-handed DNA. *Proc. Natl. Acad. Sci. USA.* 88: 4631–4635.

Lee, G. U., L. A. Chrisey, and R. J. Colton. 1994. Direct measurement of the forces between complementary strands of DNA. *Science.* 266: 771–773.

Lighthill, M. J. 1970. Fourier Analysis and Generalised Functions. Cambridge University Press, Cambridge.

Lin-Chung, P. J., and A. K. Rajagopal. 1995. Helical coordinate system and electrostatic fields of double-helix charge distributions. *Phys. Rev. E.* 52:901–906.

Lyubchenko, Y. L., A. A. Gall, L. S. Shlyakhtenko, R. E. Harrington, B. L. Jacobs, P. I. Oden, and S. M. Lindsay. 1992. Atomic force microscopy imaging of double stranded DNA and RNA. *J. Biomol. Struct. Dyn.* 10:589–606.

Lyubchenko, Y., L. Shlyakhtenko, R. Harrington, P. Oden, and S. Lindsay. 1993. Atomic force microscopy of long DNA: imaging in air and under water. *Proc. Natl. Acad. Sci. USA.* 90:2137–2140.

Manning, G. S. 1978. The molecular theory of polyelectrolyte solutions with applications to the electrostatic properties of polynucleotides. *Q. Rev. Biophys.* 2:179–246.

Mills, P., C. F. Anderson, and M. T. Record, Jr. 1985. Monte Carlo studies of counterion-DNA interactions. Comparison of the radial distribution of counterions with predictions of other polyelectrolyte theories. *J. Phys. Chem.* 89:3984–3994.

Misra, V. K., J. L. Hecht, K. A. Sharp, R. A. Friedman, and B. Honig. 1994a. Salt effects on protein-DNA interactions. The λcI repressor and endonuclease. *J. Mol. Biol.* 238:264–280.

Misra, V. K., K. A. Sharp, R. A. Friedman, and B. Honig. 1994b. Salt effects on ligand-DNA binding. Minor groove binding antibiotics. *J. Mol. Biol.* 238:245–263.

Montoro, J., C. Gil, and J. L. F. Abascal. 1995. Ionic distribution around simple DNA models. I. Cylindrically averaged properties. *J. Chem. Phys.* 103:8273–8284.

Pack, G. R., G. A. Garrett, L. Wong, and G. Lamm. 1993. The effect of a variable dielectric coefficient and finite ion size on Poisson-Boltzmann calculations of DNA-electrolyte systems. *Biophys. J.* 65:1363–1370.

Pack, G. R., and B. J. Klein. 1984. Generalized Poisson-Boltzmann calculation of the distribution of electrolyte ions around the B- and Z-conformers of DNA. *Biopolymers.* 23:2801–2823.

Pack, G. R., G. Lamm, L. Wong, and D. Clifton. 1990. The structure of the electrolyte environment of DNA. *In* Theoretical Biochemistry and Molecular Biophysics. D. L. Beveridge and R. Lavery, editors. Adenine Press, New York. 237–246.

Pack, G. R., L. Wong, and C. V. Prasad. 1986. Counterion distribution around DNA: variation with conformation and sequence. *Nucleic Acids Res.* 14:1479–1493.

Pearlman, D. A., and S. Kim. 1990. Atomic charges for DNA constituents derived from single-crystal x-ray diffraction data. *J. Mol. Biol.* 211: 171–187.

Press, W., S. Teukolsky, W. Vetterling, and B. Flannery. 1995. Numerical Recipes in C: The Art of Scientific Computing, 2nd Ed. Cambridge University Press, Cambridge.

Pullman, A., and B. Pullman. 1981. Molecular electrostatic potential of the nucleic acids. *Q. Rev. Biophys.* 14:289–380.

Rau, D. C., and V. A. Parsegian. 1992. Direct measurement of the intermolecular forces between counterion-condensed DNA double helices. Evidence for long range attractive hydration forces. *Biophys. J.* 61: 246–259.

Record, M. 1967. Electrostatic effects on polynucleotide transitions. I. Behavior at neutral pH. *Biopolymers.* 5:975–992.

Schellman, J. A. 1977. Electrical double layer, zeta potential, and electrophoretic charge of double-stranded DNA. *Biopolymers.* 16:1415–1434.

Sharp, K. A., and B. Honig. 1990a. Electrostatic interactions in macromolecules. *Annu. Rev. Biophys. Biophys. Chem.* 19:301–332.

Sharp, K. A., and B. Honig. 1990b. Calculating total electrostatic energies with the nonlinear Poisson-Boltzmann equation. *J. Phys. Chem.* 94: 7684–7692.

Shin, Y., and W. Hubbell. 1992. Determination of electrostatic potentials at biological interfaces using electron-electron double resonance. *Biophys. J.* 61:1443–1453.

Soumpasis, D. 1978. Debye-Huckel theory of model polyelectrolytes. *J. Chem. Phys.* 69:3190–3196.

Stigter, D. 1975. The charged colloidal cylinder with a Gouy double layer. *J. Colloid Interface Sci.* 53:296–306.

Stigter, D. 1995. Evaluation of the counterion condensation theory of polyelectrolytes. *Biophys. J.* 69:380–388.

Stogryn, A. 1971. Equations for calculating the dielectric constant of saline water. *IEEE Trans. Microwave Theory Tech.* 19:733–736.

Vologodskii, A., and N. Cozzarelli. 1994. Modeling of long-range electrostatic interactions in DNA. *Biopolymers.* 35:289–296.

Wang, A. H., G. J. Quigley, F. J. Kolpak, G. van Der Marel, J. H. van Boom, and A. Rich. 1981. Left-handed double helical DNA: variations in the backbone conformation. *Science.* 211:171–176.

Weisbuch, G., and M. Gueron. 1981. Polyelectrolyte theory. 3. The surface potential in mixed-salt solutions. *J. Phys. Chem.* 85:517–525.